The structural pressure dependence of potassium titanyl phosphate (KTP) to 8 GPa

1996 J. Phys.: Condens. Matter 8 2337

(http://iopscience.iop.org/0953-8984/8/14/010)

J. Phys.: Condens. Matter **8** (1996) 2337–2363. Printed in the UK

The structural pressure dependence of potassium titanyl phosphate (KTP) to 8 GPa

D R Allan† and R J Nelmes

The University of Edinburgh, Department of Physics and Astronomy, Mayfield Road, Edinburgh EH9 3JZ, UK

Received 10 October 1995

Abstract. The crystal structure of $KTiOPO_4$ (KTP) has been determined as a function of pressure to 8 GPa at ambient temperature, using single-crystal x-ray diffraction techniques. The first-order isosymmetric phase transition, at 5.8 GPa, appears to have a strong effect on the compression mechanism of the structure: in the low-pressure phase the structure compresses by polyhedral tilting *within* the cross-linking TiO_6–PO_4 chains while in the high-pressure phase relative translations and rotations of the chains themselves account for a significant proportion of the unit-cell volume reduction both at the transition and on further pressure increase. The distortion of the framework at the phase transition is accompanied by relatively large displacements of the potassium atoms to positions more closely related to the *Pnan* symmetry of the high-temperature phase. A comparison of the pressure-induced changes of the highly distorted TiO_6 octahedra with recent high-pressure optical measurements indicates that neither the lengths nor the orientations of the Ti–O bonds correlate, at least directly, with the observed variation of the second-harmonic-generating (SHG) power of the crystal. This strongly suggests that other regions of the structure may be important for the SHG properties.

1. Introduction

Among the properties required by a material to make it suitable for non-linear optic and electro-optical applications are the combination of good mechanical and thermal stability, resistance to laser damage at very high power densities, ease of growing large single-domain crystals, a wide range of transparency, and thermally stable phase-matching characteristics. Of the very few materials which meet these stringent requirements potassium titanyl phosphate, $KTiOPO_4$ (KTP), with its large non-linear coefficients and birefringence, is an extremely efficient second-harmonic generator (SHG) of Nd–YAG laser light and has become a particularly important material for an increasing number of non-linear optic applications in both the commercial and purely scientific fields. At ambient temperature and pressure, the structure of KTP assumes the acentric $Pna2_1$ space group (with lattice parameters $a = 12.819(3)$ Å, $b = 6.399(1)$ Å, $c = 10.584(2)$ Å, $V = 868.1$ Å^3 [1]) and is characterized by cross-linking chains of alternating TiO_6 octahedra and PO_4 tetrahedra, directed parallel to the a and b axes, which form a framework surrounding the K atoms. It is the highly distorted TiO_6 octahedra that have been associated with the non-linear optical properties [2] and they form additional helical chains, the direction of which alternates between $[0\,1\,1]$ and $[0\,\bar{1}\,1]$, linked by alternately long and short Ti–O bonds (as indicated in figure 1). A very considerable commercial and fundamental research effort has been

† Present address: Bayerisches Geoinstitut, Universität Bayreuth, D-95440 Bayreuth, Germany.

0953-8984/96/142337+27$19.50

expended on a search for improved SHG performance, by varying chemical composition, and this has led to the production of a whole family of structural analogues where K is substituted by (for example) Rb or Tl [3], P by As [4] and more recently where Ti is substituted by (for example) Sn [5] or Fe [6]. The structures and properties of all of these analogue materials have been reviewed in great detail [7]. Some other highly efficient SHG materials have been found, but the chemical variations make it difficult to isolate the principal structure determinants of the SHG power. A careful comparison of the variation of structure and SHG efficiency with pressure offers a 'cleaner' and potentially very effective approach.

The first measurements of the pressure dependence of KTP were undertaken by Kourouklis *et al* [8] using Raman scattering techniques. This study provided evidence of a phase transition at 5.5 GPa where an increase in the number of Raman modes was taken to indicate a lowering of the crystal symmetry, or a multiplication of the unit cell, into an antiferroelectric phase. Our more recent high-pressure structural studies of KTP to 6.2 GPa [9–11] have shown that this transition is first order in character and, surprisingly, does not lead to a change in space group. A succeeding high-pressure x-ray powder diffraction study, conducted by Somayazulu *et al* [12], has confirmed our findings. Subsequently, Tozer [13] has conducted very careful, and rather difficult, measurements of the SHG power as a function of pressure and the results of this study are depicted in figure 2. The pressure dependence is remarkably strong, with a doubling of the ambient-pressure SHG power at 2.2 GPa and then a steady decrease, followed by an abrupt fall at the transition to the high-pressure phase. Tozer's study also placed the transition pressure close to 5.8 GPa, in agreement with more recent high-pressure Raman work conducted by Serhane *et al* [14]. With the publication of these new and important results, we have collected further data to determine the pressure dependence of the high-pressure phase, and compare this with (i) the pressure dependence below the transition, (ii) the changes through the transition and (iii) how these structural changes may relate to the SHG properties.

2. The experiment and data analysis

A single crystal, of approximate dimensions 100 μm $\times$ 100 μm $\times$ 50 μm, was cut from the same bulk sample of flux-grown KTP (supplied by Dr P A Thomas of The University of Warwick) as we have used in our previous high-pressure structural studies [9–11]. Reflections measured from a series of test scans with a CAD4 four-circle diffractometer were found to give sharp diffraction peaks and, therefore, the crystal was deemed suitable for the high-pressure experiment. The crystal was mounted in a DXR-4 design of pressure cell [15] with its (1 0 0) face parallel to the diamond-anvil culets and secured in place using petroleum jelly. From our previous high-pressure studies of the structure [9–11] this orientation of the sample was found to give the lowest correlations and ESDs from refinement of the restricted data set available with the diamond-anvil pressure cell. A tungsten gasket, with a 200 μm hole, was used to enclose the sample and the ethanol–methanol pressure-transmitting fluid, and the cell taken to a pressure of 6.3 ± 0.1 GPa (measured using the ruby fluorescence method) to place the crystal into the high-pressure phase. The pressure cell was mounted on the CAD4 and the sample centred using the four-equivalent-settings procedure of King and Finger [16] with graphite-monochromated Ag Kα x-rays [17]. Test scans of selected reflections indicated that the diffraction peaks were still extremely sharp and that the crystal had remained intact and of good quality through the volume reduction at the transition.

Intensity data were collected with the ω-scan method at the position of least attenuation of the pressure cell, according to the fixed-ϕ technique [18]. All accessible reflections

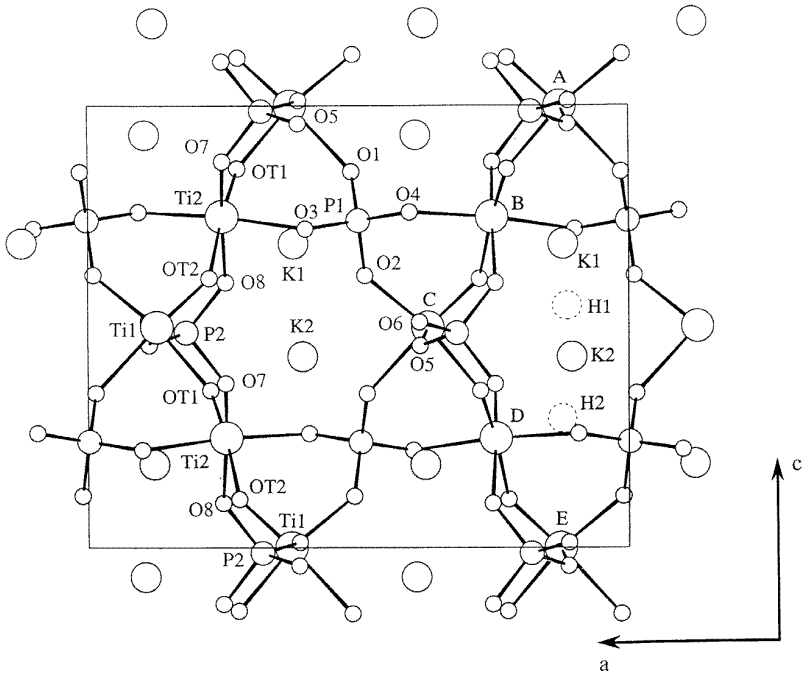

(a)

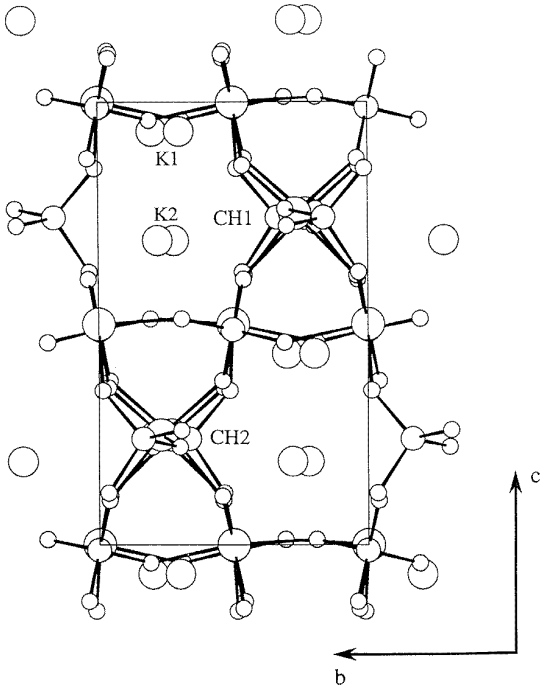

(b)

Figure 1. The structure of KTP in the low-pressure phase viewed (a) along the *b*-axis and (b) along the *a*-axis. The atoms labelled A, B, C, D, E are titanium atoms forming a chain linked by alternately long and short Ti–OT bonds.

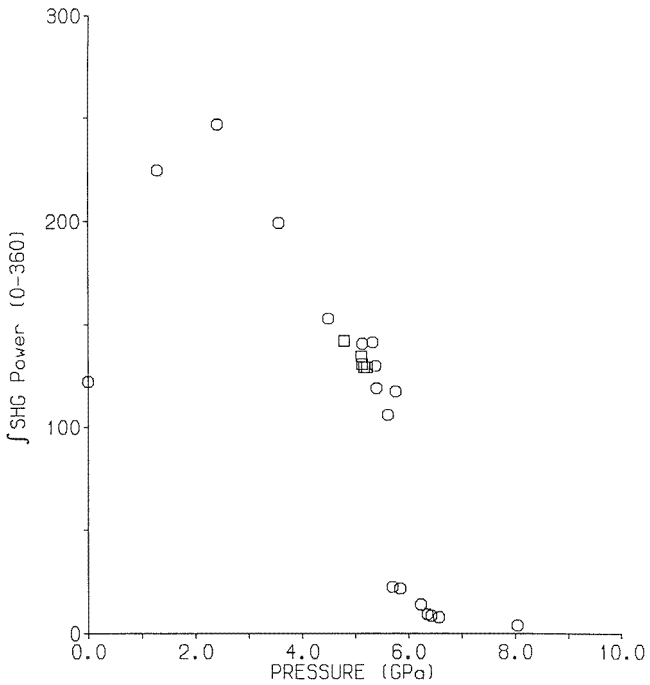

Figure 2. The integrated SHG power of KTP as a function of pressure (from the data of Tozer [13]). The circles correspond to data taken on pressure increase while the squares correspond to data taken as the pressure was decreased.

in the hemisphere $\pm h$, $\pm k$, $+1$ up to a maximum $\sin\theta/\lambda$ of 1.07 Å^{-1} were measured. After applying a correction for both pressure cell [18, 19] and sample absorption, the data were used for an initial least-squares refinement of the structure, including an extinction correction, using the Prometheus crystallographic programs [20]. The structural parameters of our first determination of the high-pressure phase [11] were used as starting values. A subset of 'leveraged' reflections [21, 22] was then identified and remeasured with increased precision. After correcting all reflections for extinction, only reflections in the original data set were averaged over symmetry equivalents so that weights could be assigned to the leveraged reflections correctly. As for our previous structural studies, in the final refinement the oxygen atoms were all refined with isotropic temperature factors while the potassium, titanium and phosphorus atoms were refined with anisotropic temperature factors (at this stage, the anisotropic thermal parameters for the atomic motion directed along [1 0 0], the direction of lowest resolution in the data, were constrained to their ambient values). Similar constraints were applied to the refinements in our previous studies [9–11] and were shown not to bias the refinement of the positional parameters significantly.

Further intensity data were collected at 8.2 GPa following the strategy already outlined for the 6.3 GPa data set and after each data collection the pressure was remeasured to ensure it had remained constant. Again the data were corrected for pressure-cell and sample absorption and the non-leveraged reflections averaged over symmetry equivalents. Additionally, the unit-cell dimensions were also determined at a pressure of 7.3 GPa using the King–Finger technique.

At this point it became apparent that the bonds which are directed nearly parallel to the

a-axis had their bondlengths determined relatively poorly. Although this was not found to be a significant problem for the study of the low-pressure phase, the large re-orientations at the phase transition lead to decreased precision on the determination of some of the key Ti–OT type bondlengths, which become less favourably oriented. It was decided, therefore, that further sets of data would be collected at 6.3 and 8.2 GPa with an alternative crystal setting. A fresh crystal was cut to the dimensions of 75 μm $\times$ 75 μm $\times$ 75 μm (from the same bulk material as used for all the previous crystals) and, after checking that it was of good quality, it was mounted in the DXR-4 cell so that the (0 0 1) face was in the plane of the diamond-anvil culets. The pressure cell was then assembled, as before, and taken to a pressure of 8.2 GPa. Following the identical alignment and intensity measurement procedures as used for the preceding setting, data were collected in the shell $0^\circ < \theta < 25^\circ$ ($\sin\theta/\lambda < 0.75$) for the hemisphere $\pm h$, $+k$, $\pm l$ and from an initial refinement a subset of leverage reflections was identified and their intensities subsequently collected to higher precision. Finally, the same experimental, intensity measurement and data reduction procedures were followed at 6.3 GPa to complete all the data sets.

The structural refinements at 6.3 and 8.2 GPa were each based on four sets of data. That is, at both pressures the data consisted of two sets of averaged reflections and two sets of leveraged reflections from each crystal setting. The data were, therefore, refined with four scale parameters and, as there was now improved resolution along the *a*-axis, the constraint on the anisotropic thermal parameters for the atomic motion directed along *a* could be relaxed.

3. Results and discussion

Table 1 presents the results from the structure refinements and the bondlengths of the K cages, Ti octahedra and P tetrahedra derived from these refinements are given in table 2. As the following discussion reviews the pressure dependence of the structure over the whole pressure range studied, 0.2–8.2 GPa, reference should also be made to the results of our previously published structural study of the low-pressure phase [10].

3.1. Unit-cell changes and volume compressibility

The unit-cell volume and relative unit-cell dimensions are plotted as a function of pressure in figures 3 and 4 respectively. The solid lines in figure 3 are Murnaghan fits to the data. For the low-pressure phase the fit gives a bulk modulus $B_0 = 58 \pm 8$ GPa with a curvature $B' = 15 \pm 4$ [10]. As the data for the high-pressure phase are limited to a range of 1.9 GPa with only three pressure points, it is not possible to yield accurate values of B_0 and B' by extrapolation to ambient pressure. Instead, the fit was performed by subtracting 5.8 GPa from each pressure value and refining an effective $B_0(B_{5.8})$ from this reduced pressure scale—thereby calculating the equation of state from the phase transition pressure. This fitting process produces values of $B_{5.8} = 75 \pm 2$ GPa and $B' = 12 \pm 3$ although, with only three data points, it is expected that the curvature is probably less well defined than the ESD suggests. In order to compare the compressibilities of the two phases at the transition, the compressibility of the low-pressure phase was determined at the transition pressure by appealing to the Murnaghan equation directly. The low-pressure phase was calculated to have $B_{5.8} = 122$ GPa and, consequently, at the phase transition the bulk modulus almost halves and the structure becomes significantly more compressible in the conformation of the high-pressure phase. A similar though smaller effect has also been observed in other framework type materials such as the minerals anorthite ($CaAl_2Si_2O_8$) and orthoenstatite

Table 1. Unit-cell dimensions (Å), unit-cell volume (Å^3) and refined fractional coordinates of KTP as a function of pressure in the high-pressure phase. The number of independent reflections (N), the number of refined parameters (n), the weighted R-factor (R_w) and the goodness of fit (Gf) are also given. The R-factor for the refinements is defined as follows:

$$R_w = \left(\left(\sum_N w(F_0 - F_c)^2 \right) \Big/ \sum_N w F_0^2 \right)^{1/2}$$

where F_0 and F_c are the observed and calculated structure factors respectively and w is the weight assigned to each reflection (in both refinements $w = 1/[\sigma^2(F_0) + 0.03]$). The goodness of fit for the refinements is given by

$$\mathrm{Gf} = \left(\left(\sum_N w(F_0 - F_c)^2 \right) \Big/ (N - n) \right)^{1/2}$$

where the symbols have the same definitions as described above. The estimated standard deviations (ESDs) for each of the values are given in parentheses. Note that symmetry requires that one atom be fixed along the polar c-axis. The Ti1 z-coordinate was chosen to be fixed and so no ESD is quoted for it.

		0.2–4.7 GPa[a]	6.3 GPa	7.3 GPa	8.2 GPa
a (Å)			12.490(6)	12.433(8)	12.387(9)
b (Å)			6.324(2)	6.314(3)	6.311(4)
c (Å)			10.069(3)	10.015(4)	9.966(5)
V (Å^3)			795.3(7)	786.2(9)	779(1)
K1	x		0.3964(3)		0.3969(3)
	y		0.7779(4)		0.7766(3)
	z		0.6309(5)		0.6321(5)
K2	x		0.1138(3)		0.1144(2)
	y		0.7013(3)		0.6999(3)
	z		0.8671(4)		0.8650(5)
Ti1	x		0.3712(2)		0.3716(2)
	y		0.4886(3)		0.4890(3)
	z		− 0.0004(0)		− 0.0004(0)
Ti2	x		0.2799(2)		0.2839(2)
	y		0.2567(2)		0.2553(3)
	z		0.7231(3)		0.7221(4)
P1	x		0.5285(3)		0.5324(3)
	y		0.3217(3)		0.3199(4)
	z		0.7603(4)		0.7638(5)
P2	x		0.1796(3)		0.1793(3)
	y		0.4811(4)		0.4791(4)
	z		0.4771(3)		0.4778(4)
O1	x		0.5158(8)		0.5208(7)
	y		0.4186(9)		0.4144(10)
	z		0.8981(8)		0.9038(10)
O2	x		0.5409(8)		0.5438(6)
	y		0.5045(11)		0.5038(10)
	z		0.6597(8)		0.6627(9)
O3	x		0.4328(8)		0.4375(7)
	y		0.1849(10)		0.1795(10)
	z		0.7130(9)		0.7165(10)

Table 1. (Continued)

		0.2–4.7 GPa[a]	6.3 GPa	7.3 GPa	8.2 GPa
O4	*x*		0.6280(8)		0.6335(6)
	y		0.1840(9)		0.1833(10)
	z		0.7565(8)		0.7583(9)
OT1	*x*		0.1883(8)		0.1831(6)
	y		0.9720(9)		0.9726(9)
	z		0.3247(8)		0.3237(8)
OT2	*x*		0.2492(9)		0.2509(7)
	y		0.0376(8)		0.0370(9)
	z		0.5782(7)		0.5740(9)
O5	*x*		0.0986(8)		0.0973(7)
	y		0.2967(9)		0.2967(9)
	z		0.4687(8)		0.4726(9)
O6	*x*		0.1225(8)		0.1233(7)
	y		0.6753(10)		0.6773(11)
	z		0.5272(9)		0.5292(10)
O7	*x*		0.2302(8)		0.2272(7)
	y		0.5125(8)		0.5085(9)
	z		0.3354(7)		0.3315(8)
O8	*x*		0.2766(9)		0.2782(8)
	y		0.4348(9)		0.4363(9)
	z		0.5649(8)		0.5652(9)
N			2823		2747
n			97		97
R_w			7.7		7.4
Gf			1.52		1.32

[a] The values for the low-pressure phase, at pressures of 0.2, 2.2, 3.7 and 4.7 GPa, are given in [10].

($MgSiO_3$) where the structures also become more compressible at pressures just above their first-order phase transitions. For anorthite B_P decreases from a value of 93.5 GPa to 85.1 GPa [23] at its $P\bar{1}$ to $I\bar{1}$ transition [24] while for orthoenstatite B_P decreases from 148.0 GPa to 144.6 GPa [25] at its isosymmetric transition (or cross-over) in the *Pbca* phase [26].

By extrapolating the Murnaghan fits of the low-pressure and high-pressure phases to the phase transition pressure (see figure 3) the volume reduction is calculated to be 2.7% (which is somewhat smaller than our previous estimate of 4.2% [11]). The volume reduction is mainly accommodated by the compression of the *c*-axis which, as can be seen in figure 4, undergoes a pronounced 2.6% contraction. The *a*-axis, on the other hand, shows a relatively smaller reduction of 0.6% while the *b*-axis *increases* slightly by about 0.4%. It is also apparent, from figure 4, that the relative rates of compression of the unit-cell axes have changed quite significantly in the high-pressure phase. Over the pressure region below the phase transition, the compression of the unit cell is approximately isotropic and the axes are reduced, on average, by about 1.8%. For the high-pressure phase, however, the compression of the unit cell is no longer so close to being isotropic and for the pressure range between

Table 2. The bond lengths (Å) of the K cages, Ti octahedra and P tetrahedra in KTP as a function of pressure in the high-pressure phase.

		0.2–4.7 GPa[a]	6.3 GPa	8.2 GPa
$K(1)O_8$	K1–O1		2.870(8)	2.769(9)
	K1–O2		2.517(10)	2.523(8)
	K1–O3		2.741(7)	2.725(8)
	K1–O5		3.404(8)	3.397(9)
	K1–O7		2.991(8)	2.908(8)
	K1–O8		2.718(8)	2.687(8)
	K1–OT1		2.945(8)	2.882(8)
	K1–OT2		2.522(9)	2.511(8)
$K(2)O_9$	K2–O1		2.715(8)	2.724(8)
	K2–O2		2.941(8)	2.886(8)
	K2–O3		3.533(9)	3.564(10)
	K2–O4		2.685(7)	2.652(7)
	K2–O5		2.842(10)	2.833(9)
	K2–O7		2.788(8)	2.785(8)
	K2–O8		2.832(9)	2.825(9)
	K2–OT1		2.898(10)	2.919(8)
	K2–OT2		2.919(9)	2.860(9)
$Ti(1)O_6$	Ti1–O1		2.121(10)	2.133(9)
	Ti1–O2		1.950(9)	1.935(9)
	Ti1–O5		2.008(6)	1.998(6)
	Ti1–O6		2.002(7)	1.990(6)
	Ti1–OT1		1.914(8)	1.882(8)
	Ti1–OT2		1.728(10)	1.716(9)
$Ti(2)O_6$	Ti2–O3		1.965(10)	1.963(9)
	Ti2–O4		1.963(10)	1.937(9)
	Ti2–O7		1.918(6)	1.906(7)
	Ti2–O8		1.952(7)	1.938(8)
	Ti2–OT1		1.749(7)	1.753(7)
	Ti2–OT2		2.048(7)	2.060(8)
$P(1)O_4$	P1–O1		1.525(8)	1.524(10)
	P1–O2		1.545(8)	1.543(8)
	P1–O3		1.550(9)	1.545(9)
	P1–O4		1.518(9)	1.522(8)
$P(2)O_4$	P2–O5		1.547(8)	1.536(8)
	P2–O6		1.507(8)	1.519(8)
	P2–O7		1.573(7)	1.585(8)
	P2–O8		1.528(10)	1.527(10)

[a] The values for the low-pressure phase, at pressures of 0.2, 2.2, 3.7 and 4.7 GPa, are given in [10].

6.3 GPa and 8.2 GPa the *a*-, *b*- and *c*-axes reduce by about 0.8, 0.2 and 1.0% respectively.

3.2. The TiO_6–PO_4 framework

The anisotropic compression of the unit cell at the transition, and the change of the compressibilities of the unit-cell axes, can be readily understood by examining the

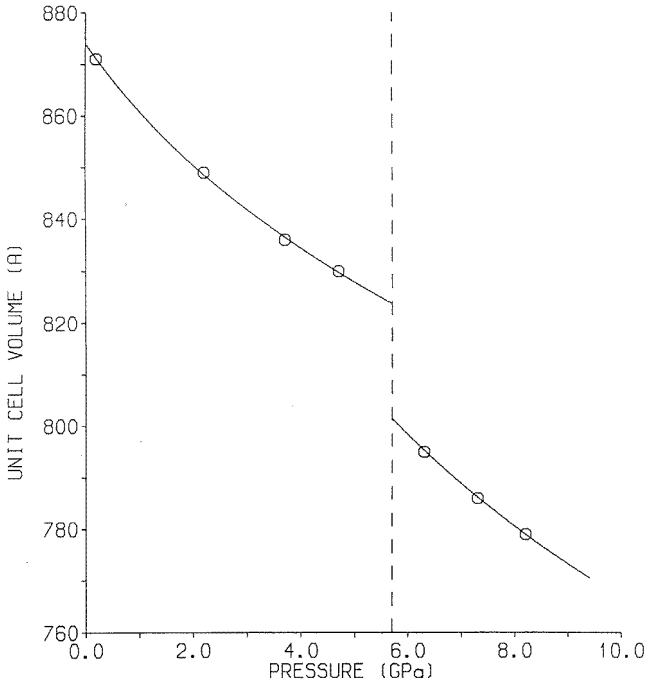

Figure 3. The unit-cell volume of KTP as a function of pressure. The errors are smaller than the symbols shown. The solid lines are fitted to the data with Murnaghan functions, as described in the text, and the dashed line indicates the phase transition pressure.

underlying changes in the crystal structure. The structure of the high-pressure phase is shown in figure 5 where the principal structural displacements have been indicated by the arrowed lines. It is apparent, from a comparison of the ambient structure (figure 1) and the high-pressure structure (figure 5), that the main structural changes at the transition involve the *n*-glide related $Ti(2)O_6$–$P(1)O_4$ chains (labelled CH1 and CH2 in figure 5), which exhibit large parallel/antiparallel translations along the *a*-axis. The cross-linking $Ti(1)O_6$–$P(2)O_4$ chains (which are directed along the *b*-axis) are rotated about the *b*-axis—half clockwise, and half anticlockwise, as illustrated in figure 5(a)—by the opposite displacements of adjacent $Ti(2)O_6$–$P(1)O_4$ chains. As there are no TiO_6–PO_4 type chains parallel to the *c*-axis to give a similar degree of stiffness as offered to the *a*- and *b*-axes by the $Ti(2)O_6$–$P(1)O_4$ and $Ti(1)O_6$–$P(2)O_4$ chains, it can be expected that these rotations will account for a significant proportion of the strong accompanying contraction of the *c*-axis at the transition and the increased relative compressibility of the structure along *c* in the high-pressure phase. This behaviour is in contrast to that observed in the $KGeOPO_4$ (KGP) structural analogue which has a relatively short *c*-axis at ambient pressure ($a = 12.6013(10)$ Å, $b = 6.3051(5)$ Å, $c = 10.0031(8)$ Å, $V = 794.8(2)$ Å^3 [27]). As the structure of KGP adopts the same structural conformation as the low-pressure phase of KTP, the contraction of the unit cell along the *c*-axis is due principally to the smaller volume of the GeO_6 octahedra compared to that of the TiO_6 octahedra. Since the average volume of the TiO_6 octahedra in KTP (calculated in the manner we have described previously [10]) decreases continuously through the transition (see table 3 and figure 6), at a rate somewhat slower than that of the unit cell, the dimensions of the TiO_6 octahedra do not appear to contribute to the *c*-axis contraction

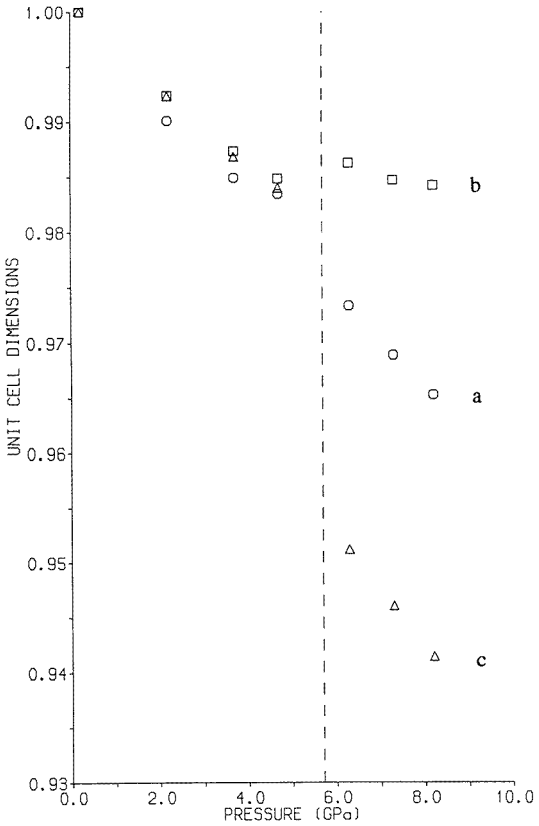

Figure 4. The pressure dependence of the unit-cell *a*-axis (○), *b*-axis (□) and *c*-axis (△) of KTP. The dashed line indicates the phase transition pressure. The errors are smaller than the symbols shown.

at the transition by such a large extent as observed in KGP. As can also be seen from figure 6, the average volume of the PO_4 tetrahedra may have a slight discontinuity at the transition, although this is small relative to the ESDs, but remains relatively unchanged over the whole pressure range studied. On the other hand, the average K-cage volume exhibits a strong pressure dependence and, as we have noted previously [10, 11], appears to absorb a significant proportion of the unit-cell compression in both the low-pressure and high-pressure phases, and also at the phase transition.

In figure 7(a), the translation of the $Ti(2)O_6$–$P(1)O_4$ chains parallel to the *a*-axis has been parametrized by the fractional coordinate change (Δx) of the P1 and Ti2 atoms. It is apparent that the translation becomes accentuated at higher pressure through the transition as is also reflected by the rotation, about the *b*-axis, of the $Ti(1)O_6$–$P(2)O_4$ chains (as has been illustrated, in figure 7(b), by plotting the angle of the Ti1–O1 and Ti1–OT2 bonds with the *c*-axis). Within the chains there are also some significant changes at the transition and, notably, the $Ti(2)O_6$–$P(1)O_4$ chains twist, as indicated by the double-headed arrows in figure 5(b). Alternate $P(1)O_4$ groups rotate by about 15° in opposite senses around the *a*-axis whilst the $Ti(2)O_6$ octahedra undergo a much smaller rotation of about 3° at the transition. These rotations are depicted in figure 8 by plotting the orientations of the P1–O2

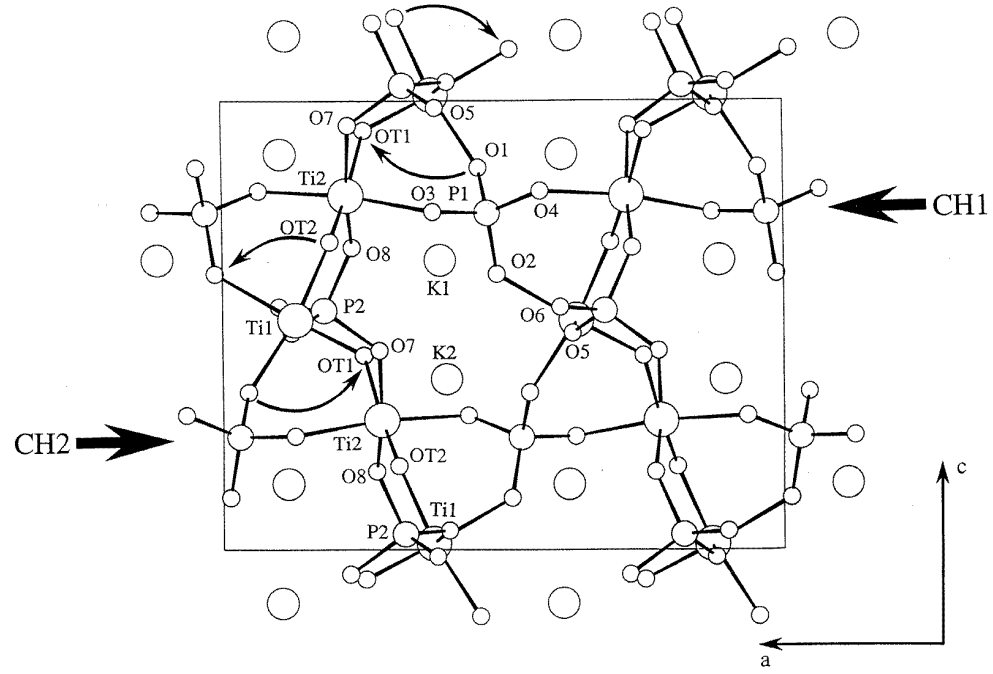

(a)

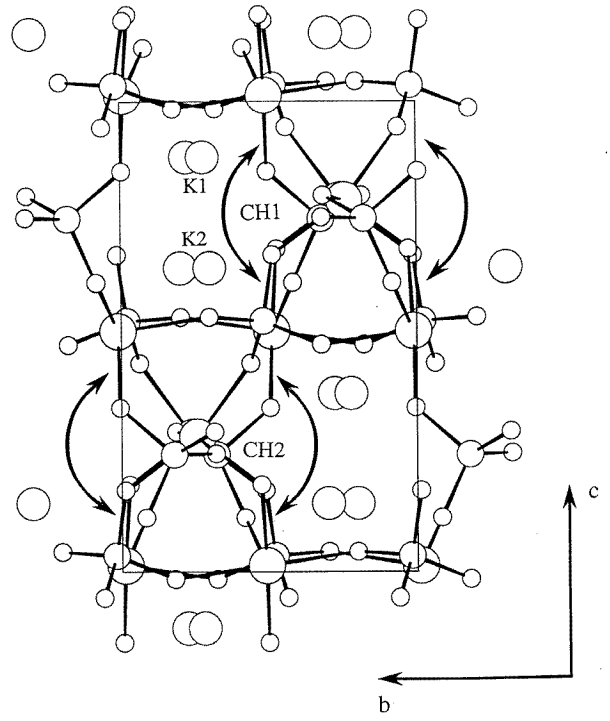

(b)

Figure 5. The structure of KTP in the high-pressure phase viewed (a) along the *b*-axis and (b) along the *a*-axis. The arrowed lines (as described in the text) indicate the major structural changes at the transition.

Table 3. The pressure dependence of the average M–O bondlengths (Å) in the TiO_6 octahedra, PO_4 tetrahedra and K cages of KTP in its high-pressure phase and the volumes (Å^3) of these structural units. The definition of the volumes is discussed in [10].

	0.2–4.7 GPa[a]	6.3 GPa	8.2 GPa
TiO_6 octahedra			
average bond length (Å)		1.943(8)	1.934(8)
volume (Å^3)		9.60(11)	9.45(11)
PO_4 tetrahedra			
average bond length (Å)		1.537(8)	1.538(9)
volume (Å^3)		1.85(3)	1.86(3)
K1 cage			
average bond length (Å)		2.838(8)	2.800(8)
volume (Å^3)		22.25(21)	21.43(21)
K2 cage			
average bond length (Å)		2.906(9)	2.894(9)
volume (Å^3)		28.64(27)	27.67(27)

[a] The values for the low-pressure phase, at pressures of 0.2, 2.2, 3.7 and 4.7 GPa, are given in [10].

Table 4. Selected P–O–Ti and Ti–OT–Ti bond angles (°) in KTP as a function of pressure. Note that most of the values, for the pressure range between 0.2 GPa and 4.7 GPa, have not been presented in our previous publications [9–11].

	0.2 GPa	2.2 GPa	3.7 GPa	4.7 GPa	6.3 GPa	8.2 GPa
P1–O1–Ti1 (°)	131.2(1.0)	130.2(8)	130.2(9)	129.0(8)	127.6(6)	125.3(5)
P1–O2–Ti1 (°)	134.0(1.0)	131.9(8)	132.2(9)	133.3(8)	127.9(5)	128.0(4)
P1–O3–Ti2 (°)	131.0(7)	129.8(7)	128.2(7)	128.1(5)	127.2(5)	126.1(4)
P1–O4–Ti2 (°)	132.9(7)	132.3(7)	131.9(7)	132.4(6)	133.3(4)	133.2(4)
P2–O5–Ti1 (°)	130.4(7)	128.7(7)	132.1(7)	131.5(5)	126.9(6)	126.6(5)
P2–O6–Ti1 (°)	136.6(9)	136.1(9)	134.8(9)	134.8(9)	137.8(6)	138.5(6)
P2–O8–Ti2 (°)	132.9(9)	130.3(9)	126.6(9)	128.9(9)	127.6(4)	126.5(4)
P2–O7–Ti2 (°)	135.0(1.0)	132.2(8)	133.4(8)	133.0(9)	126.9(6)	126.4(5)
Ti1–OT1–Ti2 (°)	135.9(9)	135.0(8)	132.4(9)	133.3(9)	132.0(4)	131.6(4)
Ti1–OT2–Ti2 (°)	134.6(9)	133.6(8)	134.3(8)	133.5(7)	127.7(5)	127.1(5)

bond, in one of the tetrahedra, and the Ti2–O8 bond, in one of the octahedra, with respect to the *c*-axis. (The P1′–O2′ and Ti2′–O8′ bonds in adjacent PO_4 tetrahedra and TiO_6 octahedra along the same $Ti(2)O_6$–$P(1)O_4$ chain are constrained by symmetry to undergo the same magnitude of rotation but in opposite senses to the P1–O2 and Ti2–O8 bonds shown in figure 8.) It appears, though, that the degree of twist in the $Ti(2)O_6$–$P(1)O_4$ chains shows no significant variation over the pressure range studied above the transition. Despite the significant twisting in the $Ti(2)O_6$–$P(1)O_4$ chain at the transition, the compression of the P1–O3–Ti2 and P1–O4–Ti2 linking bonds appears to be relatively continuous across the full pressure range (as can be seen in figure 9 and table 4). It is particularly significant that these linking bonds, of which the P1–O3–Ti2 exhibits one of the largest pressure-induced changes in the low-pressure phase [10], appear to have the same pressure dependence both above and below the phase transition. For the $Ti(1)O_6$–$P(2)O_4$ chains, the P2–O5–Ti1 and

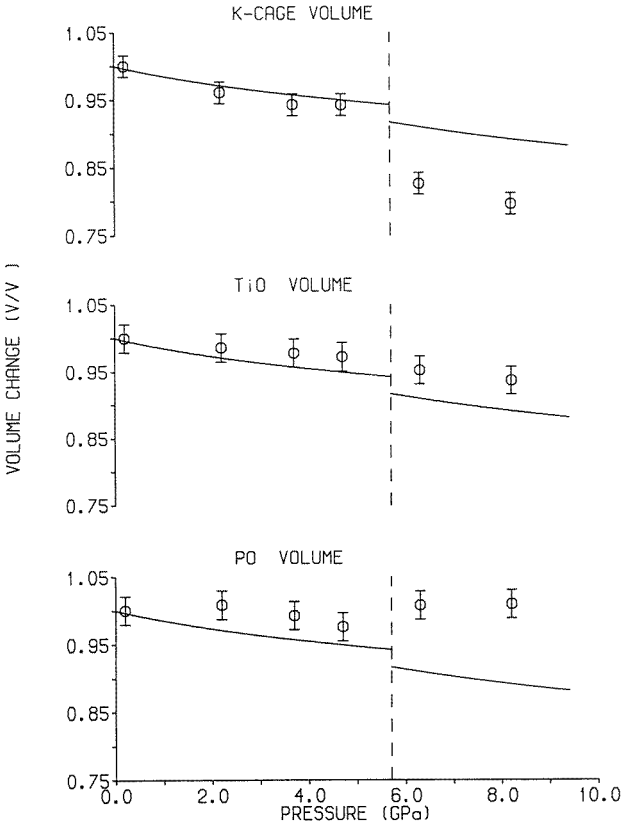

Figure 6. The relative volumes (V/V_0) of the K cages (the K1 and K2 cages averaged), the TiO_6 octahedra and the PO_4 tetrahedra in KTP as a function of pressure, referred to the value V_0 at 0.2 GPa. The solid lines are from Murnaghan fits to the relative volume of the unit cell and are a guide to the eye. The dashed line indicates the phase transition pressure.

P2–O6–Ti1 bond angles both appear to undergo a discontinuous change at the transition (figure 9, table 4), although the spread of the points makes the pressure dependence of the P2–O5–Ti1 linking bond in the low-pressure phase less well determined.

The pressure dependences of the P–O–Ti type bonds, linking neighbouring $Ti(1)O_6$–$P(2)O_4$ and $Ti(2)O_6$–$P(1)O_4$ chains, are shown in figure 10(a) and are presented in table 4. It is apparent that all the bond angles reduce, or become more acute, over the whole pressure range but at the phase transition the bonds appear to exhibit two distinctly different types of behaviour. The P1–O1–Ti1 and P2–O7–Ti2 linking bonds both appear to vary continuously through the phase transition while the P1–O2–Ti1 and P2–O8–Ti2 linking bonds show large and very abrupt bond angle reductions. This behaviour is also reflected in the Ti1–OT1–Ti2 and Ti1–OT2–Ti2 bonds, which link adjacent TiO_6 octahedra to form the characteristic helical chains, as can be seen in figure 10(b). The Ti1–OT2–Ti2 bond shows an abrupt change of about 6° at the transition while the Ti1–OT2–Ti2 bond appears to reduce continuously both below and through the phase transition. As all of these bonds form links between the translating $Ti(2)O_6$–$P(1)O_4$ chains and the rotating $Ti(1)O_6$–$P(2)O_4$ chains, which both reorient very abruptly at the transition, the continuous variation of some

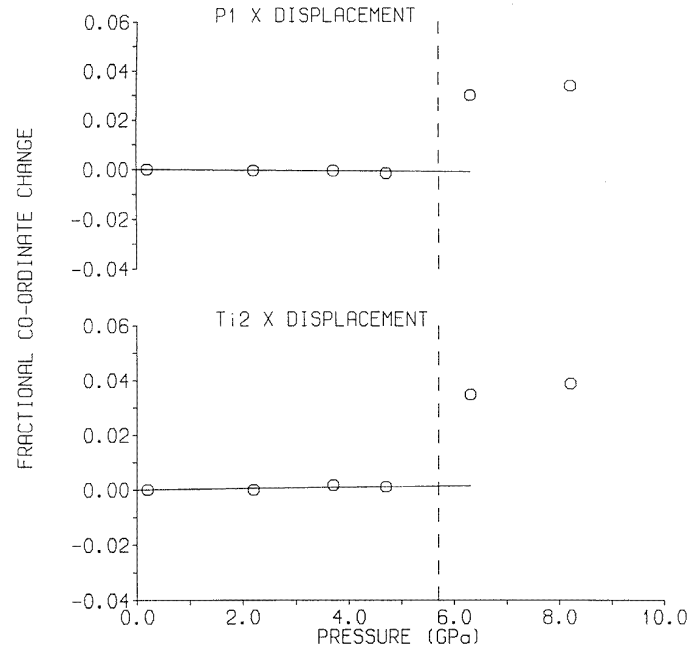

(a)

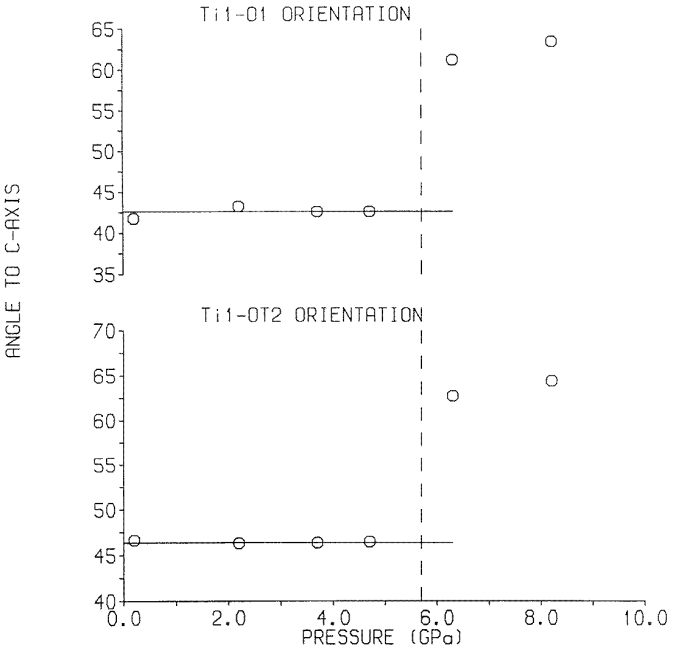

(b)

Figure 7. (a) The fractional coordinate change along the *a*-axis of the P1 and Ti2 atoms in KTP as a function of pressure. (b) The angles subtended by the Ti1–O1 and Ti1–OT2 bonds with the *c*-axis in $KTiOPO_4$. In both (a) and (b), the dashed lines show the phase transition pressure and the errors are smaller than the symbols shown. The solid lines are a guide to the eye only.

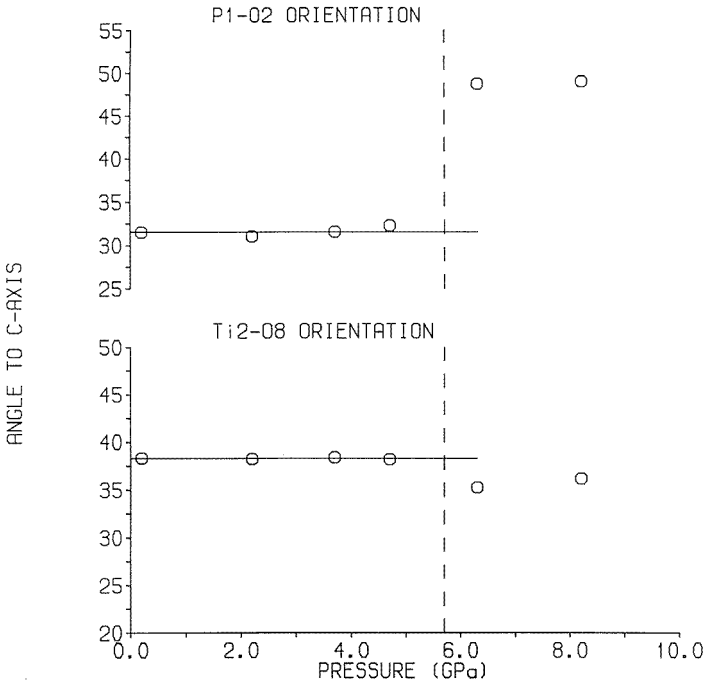

Figure 8. The angles subtended by the P1–O2 and Ti2–O8 bonds with the *c*-axis in KTP. The errors are smaller than the symbols shown and the dashed lines indicate the phase transition pressure. The solid lines are a guide to the eye only.

of the bonds may be due in part to the twisting of the $Ti(2)O_6$–$P(1)O_4$ chains, and some substantial bond angle changes *within* the $Ti(2)O_6$ octahedra, that preserve the P–O–Ti bond angles through the transition. For example, the O7–Ti2–OT1 bond angle increases by approximately 11° at the transition while the O8–Ti2–OT2 and O7–Ti2–OT2 bonds both have angular changes of about 5°. The $Ti(1)O_6$ octahedra, in contrast, appear to be much more rigid and the intra-octahedral bond angles change by no more than about 2° at the transition. As is suggested by their relative incompressibility, the PO_4 groups also appear to remain very rigid and the intra-tetrahedral bond angles, O–P1–O and O–P2–O, change by less than 2° between 4.7 GPa and 6.3 GPa.

3.3. The K-cage sites

The substantial buckling of the TiO_6–PO_4 framework at the transition leads to the relatively large, approximately 12%, volume collapse of the K-cage sites. This compression is accompanied by significant movements of the potassium atoms themselves, mainly along the polar *c*-axis, as shown in figure 11. These movements may be related, in part, to the *Pnan* pseudo-symmetry of the ambient-pressure structure [1] which is derived from the space group symmetry of the high-temperature phase (which the structure adopts through a second-order transition at 934 °C [1, 28]). The movements of the potassium atoms, which are of the order of 0.5 Å with respect to the TiO_6–PO_4 framework, correspond to K1 and K2 adopting positions that are closely *n*-glide related: i.e. if the pseudo-*n*-glide, through $z = 0$, were present there would be only one independent potassium atom described by the average

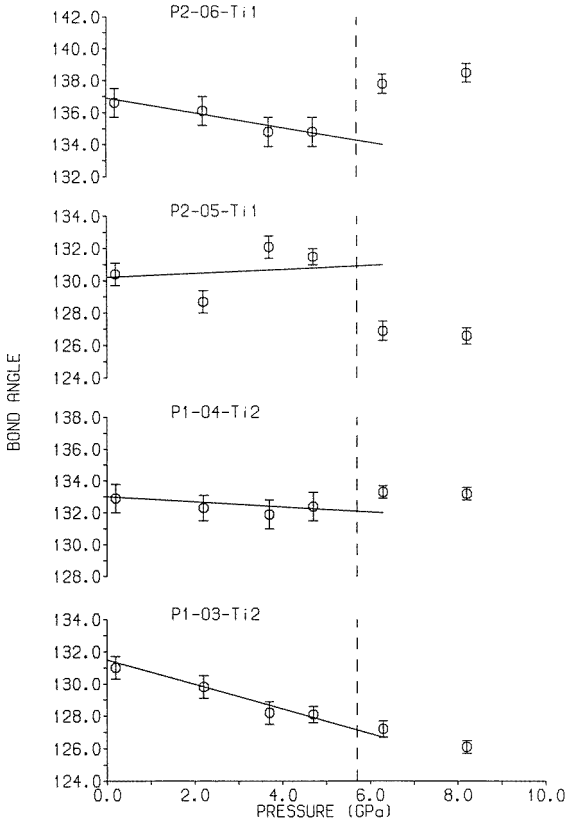

Figure 9. The pressure dependence of the linking bond angles in the $P(1)O_4$–$Ti(2)O_6$ and $P(2)O_4$–$Ti(1)O_6$ chains of KTP. The dashed lines indicate the phase transition pressure. The solid lines are a guide to the eye.

of the K1 and K2 positions [29]. The distance, Δ, between the K2 atomic position and the pseudo-*n*-glide-related K1 atomic position is given in table 5, and plotted in figure 12, for the full pressure range studied. It is apparent that the distance between the pseudo-*n*-glide-related K1 and K2 positions decreases slightly, by about 4%, as the phase transition is approached but reduces very abruptly, by about 85%, at the transition. Much of the reduction at the transition can be attributed to the shifts of both the K1 and K2 atoms along the *c*-axis, as has already been mentioned. This significantly decreases the Δ_z displacement of the potassium atoms which make the largest contribution to the 'distortion' away from the *Pnan* pseudo-symmetry of the whole low-pressure structure [1]. In contrast, the framework atoms of the high-pressure structure adopt positions that generally increase the distortion from the *Pnan* pseudo-symmetry. For example, the distance, Δ, for pseudo-*n*-glide-related Ti2 atoms increases from 0.255 Å at 4.7 GPa to 0.927 Å at 6.3 GPa. This increase can be attributed almost exclusively to the large parallel/antiparallel shifts of the $Ti(2)O_6$–$P(1)O_4$ chains with respect to the *a*-axis. It appears, then, that at least the potassium atoms move towards their *Pnan* type positions in the high-pressure phase.

As the structure retains the $Pna2_1$ symmetry at the phase transition, the underlying *Pnan* pseudo-symmetry of the low-pressure phase can have no direct influence on the structural

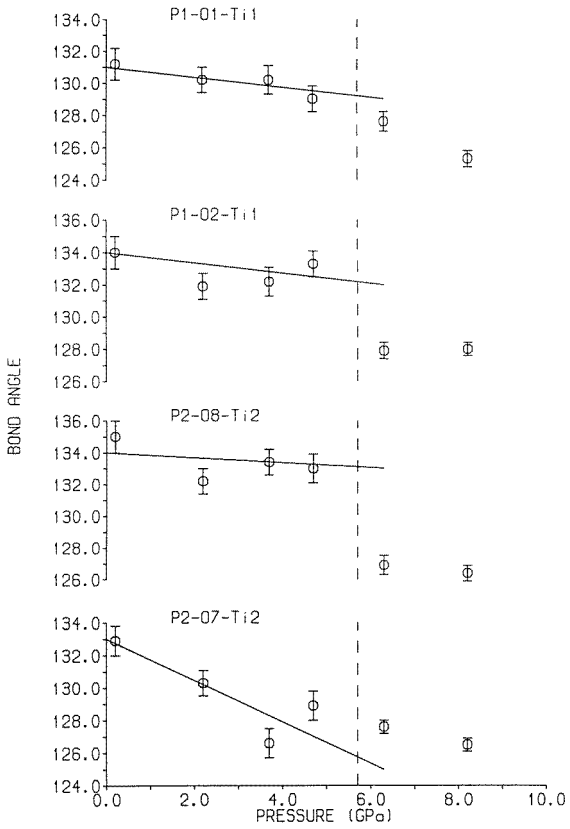

Figure 10. (a) Selected P–O–Ti linking bond angles in KTP as a function of pressure. The dashed lines indicate the phase transition pressure. The solid lines are a guide to the eye.

Table 5. The displacements Δx, Δy, Δz (Å) of the K2 atomic position from the pseudo-*n*-glide-related K1 atomic position with respect to the crystallographic axes. The distance Δ (Å) between these positions is calculated from

$$\Delta = (\Delta_x^2 + \Delta_y^2 + \Delta_z^2)^{1/2}.$$

The calculations have assumed a pseudo-*n*-glide through $z = 0$.

	0.2 GPa	2.2 GPa	3.7 GPa	4.7 GPa	6.3 GPa	8.2 GPa
Δx (Å)	−0.2002	−0.1753	−0.1769	−0.1716	0.1274	0.1400
Δy (Å)	−0.1359	−0.1642	−0.1722	−0.1705	−0.1315	−0.1483
Δz (Å)	1.2682	1.2448	1.2401	1.2219	−0.0201	−0.0289
Δ (Å)	1.291	1.268	1.264	1.246	0.184	0.206

changes and the movement of the potassium atoms to more *Pnan*-related positions could be considered as being purely coincidental. However, a possible explanation for the behaviour of the potassium atoms may be found from the recent identification of 'hole sites' in the ambient KTP structure [30]. From a close examination of the structural parameters, it was found that each potassium atom is highly asymmetrically coordinated by oxygen atoms and that at a short distance (about 1.5 Å) along $-c$ from each potassium atom there is a vacant

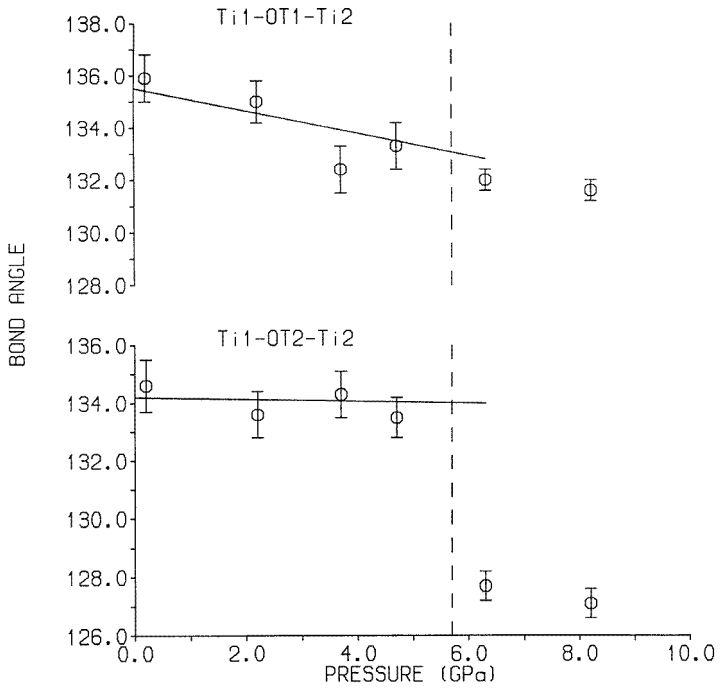

Figure 10. (b) Selected Ti–OT–Ti linking bond angles in KTP as a function of pressure. The dashed lines indicate the phase transition pressure. The solid lines are a guide to the eye.

site, a hole site (H1 and H2 in figure 1), of similar size and oxygen coordination to the K site. In the high-temperature phase the presence of the *n*-glide plane causes the pseudo-symmetrically related K1 and H1 (K2 and H2) sites to merge together along [0 0 1] at the average high-temperature potassium atom position. This new K site would be characterized by the absence of the large 'hole' region present in the ambient structure. Although a different behaviour is to be expected at high pressure, the smaller K-cage volumes of the high-pressure phase also correspond to an absence of the hole sites as does the accompanying shift of the potassium atoms to positions more closely related to the pseudo-symmetry [29].

3.4. The SHG properties

With the recent publication of Tozer's [13] results, it is now particularly important to examine whether there are any pressure-induced structural changes that may correlate with the variations observed in the SHG efficiency as a function of pressure. As it is the highly distorted TiO_6 octahedra that have been linked most closely with the SHG properties of the crystal, it is this part of the structure that will be examined in most detail.

The bondlengths of the opposing Ti1–OT1, Ti2–OT1 and Ti1–OT2, Ti2–OT2 bonds are presented in figure 13(a) and (b) respectively. In the low-pressure phase, as we have previously noted [10], it is the Ti1–OT2 and Ti2–OT2 bonds that show the largest variations with pressure. The longer of the two, Ti2–OT2, clearly reduces in length while the shorter one, Ti1–OT2, appears to increase slightly. These changes reduce the difference between the bondlengths by about 20% as the phase transition is approached. The Ti1–OT1 and Ti2–OT1 bonds, on the other hand, show very little variation between 0.2 GPa and 4.7 GPa

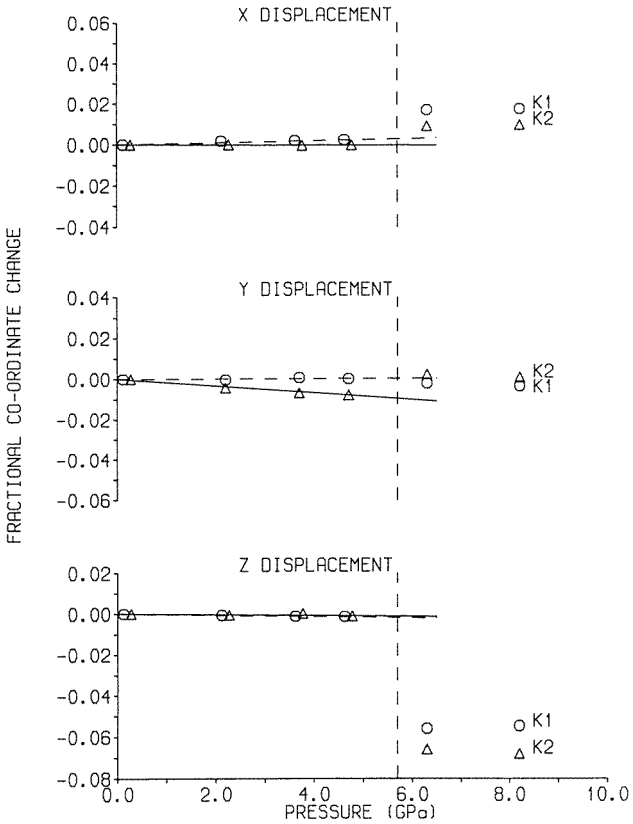

Figure 11. Fractional coordinate changes for the K1 (○) and K2 (△) atoms in KTP relative to the 0.2 GPa values. Some of the points have been translated slightly along the pressure axis to avoid overlap. The dashed and solid lines through the points represent the movements of the K1 and K2 atoms respectively in the low-pressure phase, and are a guide to the eye only. The vertical dashed lines indicate the phase transition pressure.

and their bondlength difference appears to be retained. At the phase transition, it is only the Ti1–OT1 bond that exhibits any significant discontinuity (with its bondlength reducing by about 3%) while the other Ti–OT type bonds vary nearly continuously through the transition. There is also some suggestion that the trend in the pressure dependence of these bonds may be reversed as the structure crosses from the structural conformation of the low-pressure phase into that of the high-pressure phase. It is significant, however, that the anomalously short bonds, Ti1–OT2 and Ti2–OT1, which have been most closely associated with the SHG properties of the crystal, do not show an abrupt length variation at the transition that might be expected from the sharp fall in the SHG efficiency observed by Tozer [13] (see figure 2). It is interesting to note, though, that the large peak in the SHG output power, close to 2.2 GPa, appears to bear some correlation to the very slight curvature in the pressure-dependent variation of these bondlengths (figure 13). Given that the present study only shows a deviation from non-linearity in the order of 1σ at most, the evidence for such a relationship is fairly weak and the structural pressure dependence of the low-pressure phase will need to be determined with significantly greater precision to establish whether or not a correlation exists.

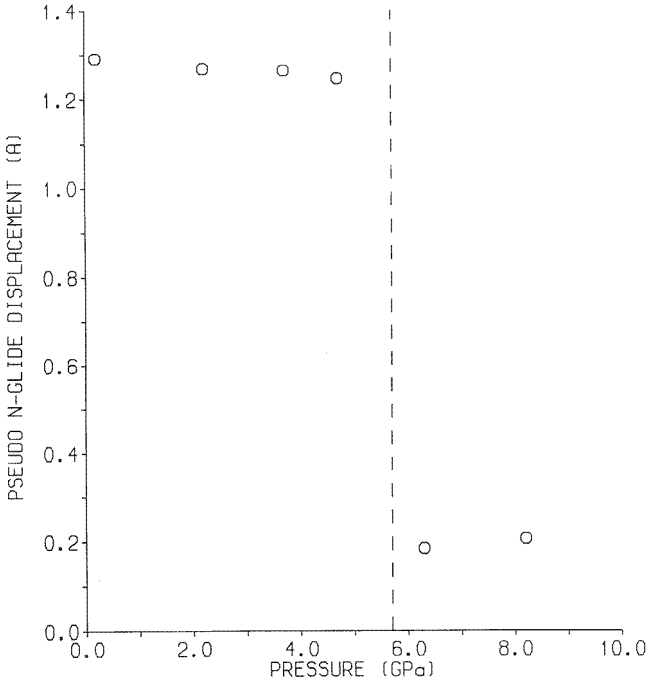

Figure 12. The displacement (Å) of the K2 atomic position from the pseudo-*n*-glide-related K1 atomic position. The dashed line indicates the phase transition pressure.

In the recent review article by Stucky *et al* [7], the component of the non-linear polarizability along the O–Ti–O octahedral axis, β_{333} (taken to be parallel to O1–Ti1–OT2 and OT1–Ti2–OT2 in the Ti(1)O_6 and Ti(2)O_6 octahedra respectively), was calculated from a model based on orbital mixing for an MO_6 octahedron with variable geometry. The distortion of the octahedra was parametrized as the difference, $2\Delta'$, between the two *trans*-Ti–O bonds parallel to the octahedral axis and the average, R_{av}, of the two equilibrium Ti–O distances. The model indicates that there is a maximum in the hyperpolarizability for certain values of $2\Delta'$, dependent upon R_{av}, and for large enough distortions there is a change of sign. Figure 14 presents the difference, $2\Delta'$ between the Ti1–O1, Ti1–OT2 (Δ'(O1–OT2)) and the Ti2–OT1, Ti2–OT2 (Δ(OT1–OT2)) bonds respectively along with the average value of β_{333} determined from these bondlength differences. The value of β_{333} for each pressure was estimated by interpolating between the curves calculated by Stucky *et al* [7] and the error bars are expected to be a reasonable assessment of the uncertainties involved in this process. The values of R_{av} at each pressure are calculated from the average of the Ti1–O1, Ti1–OT2 and the Ti2–OT1, Ti2–OT2 bondlengths. It is apparent, from figure 14, that both Δ'(O1–OT2) and Δ'(O1–OT2) decrease with pressure as the phase transition is approached and there is an apparent accompanying increase in β_{333}. This increase, though, is relatively small compared to the ESDs and there is certainly no evidence of a peak in β_{333} that might correlate with the peak observed in the SHG power at 2.2 GPa (see figure 2). At the phase transition, it is unclear whether there is a discontinuity in either the bondlength differences, Δ', or β_{333} and, again, if some form of correlation is expected with the SHG efficiency, a strong discontinuity ought to be observed. It is also apparent that, in the high-pressure

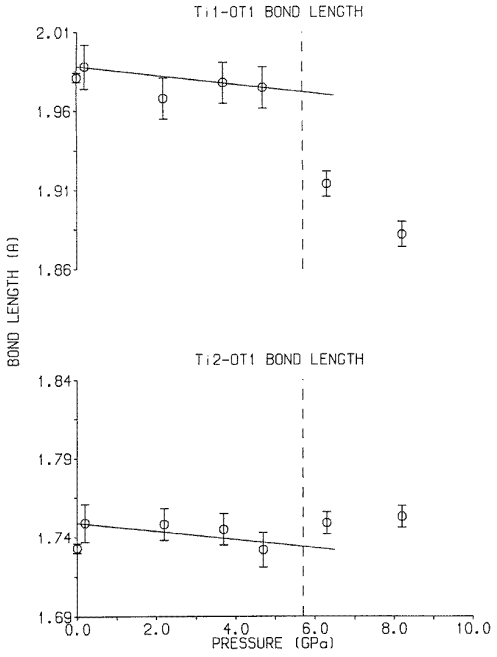

(a)

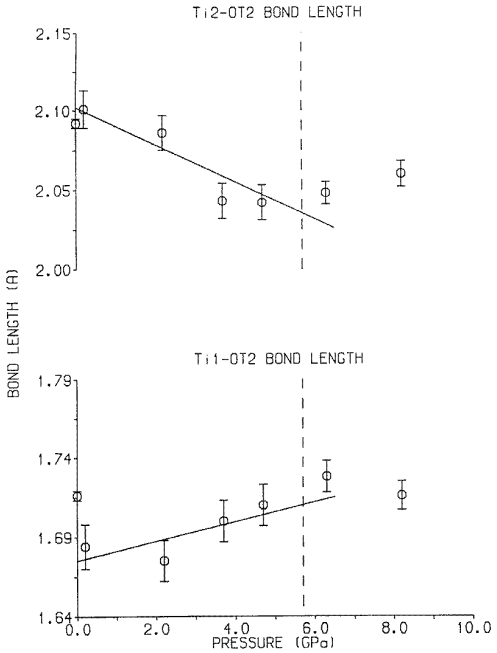

(b)

Figure 13. (a) The Ti1–OT1 and Ti2–OT1 and (b) the Ti2–OT2 and Ti1–OT2 bondlengths in KTP as a function of pressure. The solid lines are a guide to the eye only and indicate the changes in the bonds in the low-pressure phase. The phase transition pressure is indicated by the vertical dashed lines.

phase, as was observed for the Ti–OT bonds, the pressure dependence, or trends, of the low-pressure phase appear to be reversed. More recent calculations by Munowitz *et al* [31], based on a similar model of a distorted TiO_6 octahedron, also show that there is a strong dependence of β_{333} on Δ'. However, as for our comparison with the data of Stucky *et al*, the observed variation of Δ' with pressure would correspond to only a small variation in β_{333} which would not correlate with the pressure dependence of the SHG power.

The orientation of the Ti–O bonds, as well as the variation of their bondlengths, is also considered to be important for the non-linear optical properties of the KTP structure [1, 32, 33]. In the calculation of the geometrical contribution of the structure to the non-linear tensor coefficients, the orientations of the bonds participate through products of their direction cosines. Briefly summarized, a tensor component of the second-order susceptibility is given by

$$d_{ijk} = \sum_{b}^{cell} g_{ijk}^{b} \beta^{b} / V$$

where V is the volume of the unit cell, β^b is the longitudinal bond polarizability of the bth bond (with the transverse component set to zero) and the g_{ijk}^b term for a bond is given by

$$g_{ijk}^{b} = \cos(\nu_i)\cos(\nu_j)\cos(\nu_k)$$

where the direction cosines are calculated with respect to the crystallographic axes. For the KTP structure there is a strong inherent asymmetry in the summation over the g_{ijk}^b terms due to the presence of the long and short Ti–O bonds in the highly distorted TiO_6 octahedra. In the calculations performed by Hansen *et al* [32], this asymmetry was exploited by including only five of the six Ti–O bonds in each octahedron (omitting the Ti1–O1 and Ti2–OT2 bonds) and assigning the anomalously short Ti–OT bonds as higher contributors. With this approach, the tensor component d_{333} is given by a two-term equation of the form

$$d_{333} = [-2.34\beta^{(1)} + 1.64\beta^{(2)}]/V$$

where $\beta^{(1)}$ and $\beta^{(2)}$ refer to the bond polarizabilities of the short and medium-length Ti–O bonds respectively, neglecting the K–O and the P–O bonds which are not expected to contribute significantly [34]. From experimentally determined values of the single-crystal d_{ijk}, Hansen *et al* [32] calculated that $\beta^{(1)} = 14\beta^{(2)}$ and, therefore, the contribution of the anomalously short bonds to d_{333} is significantly greater than the other bonds in the TiO_6 octahedra.

In figure 15, the orientations of the anomalously short bonds (Ti1–OT2 and Ti2–OT1), with respect to the c-axis, have been plotted along with the pre-multiplier of the $\beta^{(1)}$ term (labelled g_{333}). As the phase transition is approached, the bond orientations and the g_{333} term appear to remain constant and at the transition there is an abrupt reorientation of both the Ti1–OT2 and Ti2–OT1 bonds which is accompanied by a sharp, approximately 50%, reduction in the g_{333} term. In the high-pressure phase the increasing distortion of the structure, between 6.3 GPa and 8.2 GPa, results in the progressive reorientation of the bonds and a continued reduction of the geometrical g_{333} component. If the pressure dependence of the g_{333} term is compared with Tozer's measurements of the vartiation of the SHG efficiency with pressure [13] (see figure 2), it appears that the peak in the SHG performance at 2.2 GPa does not correlate, at least directly, with g_{333}. It is also apparent that the 50% reduction of g_{333} at the phase transition is somewhat less than the 80% decrease of the SHG output power. As the lengths of both the Ti1–OT2 and Ti2–OT1 bonds remain constant at the transition, this discrepancy cannot be readily explained if it is assumed that it is mainly these anomalously short bonds that make a significant contribution to the SHG performance

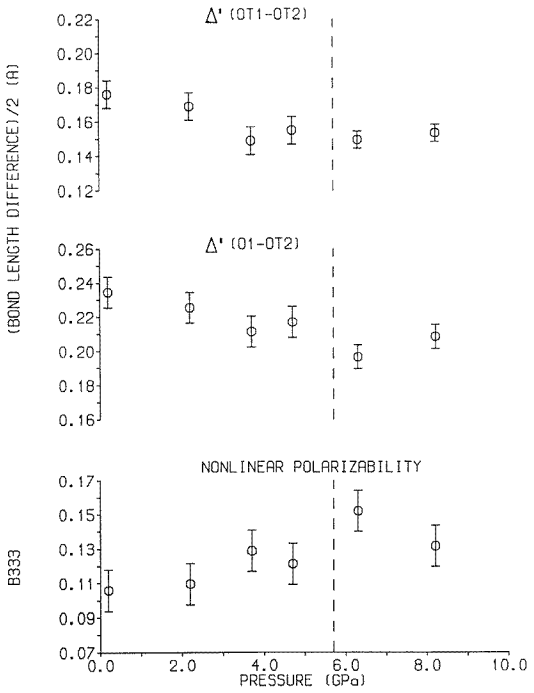

Figure 14. The Ti2–OT1 and Ti2–OT2 and the Ti1–O1 and Ti1–OT2 bondlength differences (Δ') in KTP as a function of pressure. The lower graph shows the variation in the average non-linear polarizability (β_{333}) accompanying the changes in the bondlength differences, as described in the text. The dashed lines indicate the phase transition pressure.

of the crystal. Nevertheless, the behaviour of the g_{333} term does suggest that the orientation of the bonds is important.

There are also some other significant Ti–O bondlength changes at the transition and, for example, the Ti1–O6 bond increases by about 2% while the Ti2–O3 bondlength shows a marked decrease of about 3%. These bonds are associated with the P2–O6–Ti1 and P1–O3–Ti2 linking bonds which connect the $P(2)O_4$–$Ti(1)O_6$ and $P(1)O_4$–$Ti(2)O_6$ chains along the *b*- and *a*-axes respectively. All the other Ti–O type bonds show changes of around 1.5%, or less, at the transition. The pre-multiplier of $\beta^{(2)}$, which contains the geometrical component of the medium-length bonds (excluding Ti1–O1 and Ti2–OT2), shows a marked 30% *increase* at the transition so further limiting the contribution of the TiO_6 octahedra to the observed decrease of the SHG efficiency at the phase transition.

Finally, it is also worth noting that there has been some recent interest in the link between the Ti1–OT1–Ti2 bond angle and the SHG properties. In their study of the sodium-doped analogue material $Na_xK_{1-x}TiOPO_4$ (NaKTP) Crennell *et al* [35] observed that with a stoichiometry of $x = 0.5$ the non-linear optical (NLO) properties and framework structure were essentially unchanged from those of KTP. In the β-$NaTiOPO_4$ (NaTP) end member, however, the NLO coefficient is an order of magnitude inferior and it was proposed that a structural parameter correlating with the trend in the NLO properties would exhibit only a small variation between KTP and NaKTP but would, presumably, show a significant change for NaTP. The only structural parameter that was found to satisfy this condition was the Ti1–OT1–Ti2 bond angle, which is 134.4° in NaKTP, compared with 135.5° and 130.8°

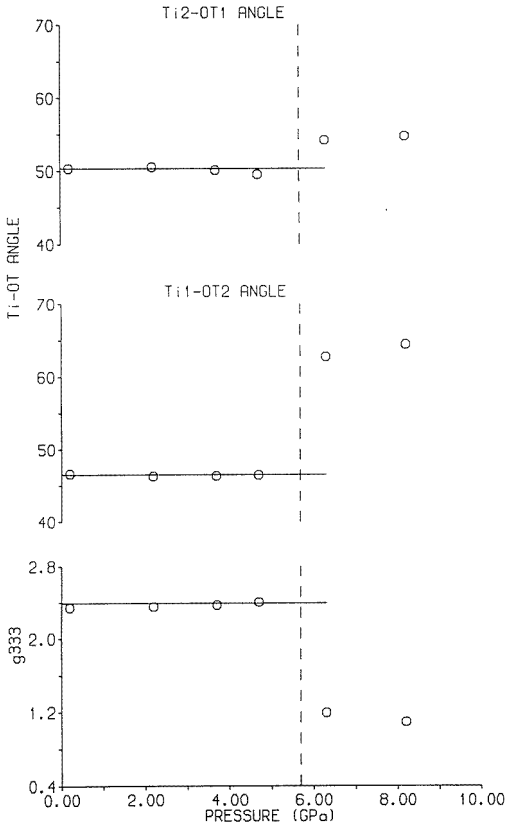

Figure 15. The pressure dependence of the orientations of the anomalously short Ti2–OT1 and Ti1–OT2 bonds with respect to the *c*-axis and the accompanying variation of their geometrical contribution (g_{333}) to the second-order susceptibility. The errors are smaller than the symbols shown. The solid lines show the pressure dependence in the low-pressure phase and are guides to the eye only. The dashed lines indicate the phase transition pressure.

in KTP and NaTP respectively. More recently Munowitz *et al* [36] have repeated these measurements and performed calculations to predict the effects of the Ti1–OT1–Ti2 bond angle on the SHG properties. Their measurements revealed a similar trend to that observed by Crennell *et al* but with a smaller intensity fall—the intensity relative to KTP falling from 0.81 ($x = 0.5$) to 0.68 ($x = 1$). These results were found to be broadly consistent with the theoretical calculations which predicted that there should be a correlation between the SHG efficiency and the Ti1–OT1–Ti2 angle. Over the pressure range we have studied, the Ti1–OT1–Ti2 linking bond angle in KTP decreases continuously by 4.3° (see figure 10(b)) and this is of a similar magnitude to the 3.6° decrease between NaKTP and NaTP. Although the fall in the SHG efficiency over this pressure range is somewhat larger than would be expected from the model of Munowitz *et al* for the corresponding bond angle changes in KTP, the overall trend gives some support to the suggestion that there is a link between the Ti1–OT1–Ti2 bond angle and the SHG properties of the crystal. However, as the peak in the pressure dependence of the SHG output power and the discontinuity at the transition (figure 2) are not reflected in the variation of this bond angle, the link can only be, at best,

indirect.

4. Summary and conclusions

The principal pressure-induced changes of the KTP structure appear to be related to the relatively compressible potassium-cage sites which were found to absorb a significant proportion of the unit-cell volume reduction. As the phase transition is approached the PO_4 and TiO_6 units remain rigid in size and shape, and the compression of the cages appears to be accommodated by significant buckling of the framework structure [10]. The phase transition was found to be strongly first order and characterized by large parallel/antiparallel translations of the *n*-glide-related $Ti(2)O_6$–$P(1)O_4$ chains, accompanied by rotations of the $Ti(1)O_6$–$P(2)O_4$ chains about an axis parallel to [0 1 0]. These relatively large changes within the framework were found to increase the compressibility of the structure from $B_{5.8} = 122$ GPa to $B_{5.8} = 75.2$ GPa at the phase transition pressure. The compression of the structure in the high-pressure phase was found to involve mainly an increase of the structural distortions induced by the phase transition: the $Ti(2)O_6$–$P(1)O_4$ translations become accentuated at higher pressure and the $Ti(1)O_6$–$P(2)O_4$ chains increase the magnitude of their rotation about the *b*-axis. Within the $Ti(2)O_6$–$P(1)O_4$ chains there appears to be significant twisting: alternate PO_4 groups rotate in opposite senses around the *a*-axis. The twist, and the large accompanying inter-octahedral O–Ti2–O bond angle changes, appear to preserve some of the cross-linking P–O–Ti linking bond angles through the transition. The potassium atoms were also found to show very large displacements at the phase transition. These displacements were found to move the potassium atoms to positions more closely related to the *Pnan* pseudo-symmetry and, therefore, the behaviour of the potassium atoms appears to be related to the merging of the K sites with the pseudo-symmetrically related 'hole' sites.

The peak in the SHG efficiency, observed by Tozer [13], at 2.2 GPa does not correlate, at least directly, with either the anomalously short Ti–OT bondlengths or the non-linear polarizability of the TiO_6 octahedra (as defined by Stucky *et al* [7]). Although the pronounced reduction of the geometrical contribution of the anomalously short Ti–OT bonds may partly explain the abrupt fall in the SHG efficiency at the transition, the lack of any clear link between the pressure dependence of the TiO_6 octahedra and the SHG properties strongly suggests that other structural variations are important and now need to be identified. Certainly, as the current high-pressure structural data have only two points covering the range from 0.2 GPa to the peak in the SHG efficiency at 2.2 GPa, a more detailed determination of the pressure dependence of the low-pressure phase is also required.

KTP has attracted a great deal of scientific and commercial attention due to its superior non-linear optical properties and our identification of a high-pressure isosymmetric phase transition has led to a new interest in the material for the study, and understanding, of the underlying mechanisms of such transitions [37, 38]. This has become particularly important with the recent identification of similar phase transitions in other framework-type materials. For example, the high-pressure single-crystal x-ray diffraction study of the mineral orthoenstatite ($MgSiO_3$), by Hugh-Jones and Angel [26], revealed that the volume variation with pressure was best described by two independent equations of state for pressures above and below $\sim$ 4 GPa. The alteration of the equation of state was found to be due to an abrupt change in the compression mechanism of the structure. At pressures below $\sim$ 4 GPa the structural compression is accommodated by changes in the conformation of the chains of essentially rigid corner-sharing SiO_4 tetrahedra, but at higher pressures there is in addition significant compression of the Si–O tetrahedral bonds. The

abrupt change in both the equation of state and the compression mechanism is strongly suggestive of a first-order isosymmetric phase transition, although the volume reduction at 4 GPa is somewhat small, about 0.7 $Å^3$ per cell, and is of the order of the experimental uncertainties. Other framework minerals such as anorthite ($CaAl_2Si_2O_8$) [24, 39], amazonite microcline ($KAlSi_3O_8$) [24, 40] and some pyroxene structures [41, 42] show evidence for similar changes under pressure, and we believe that this is probably a general phenomenon in complex framework type structures which have enough structural degrees of freedom to allow changes in compression mechanism. For the materials studied so far at high pressure with single-crystal x-ray diffraction techniques, such as orthoenstatite, the changes have been fairly subtle and have only been identified through very detailed and careful work. As the phase transition in KTP is particularly strong, and the structural changes are relatively large, the family of KTP type structural analogues could become an important class of materials for the study of these isosymmetric transitions.

Finally, it is also interesting to note that, although the compression of the K-cage site has an important role in the pressure dependence of the structure, substitution of an alternative atomic species for potassium appears to have only a limited effect on the phase transition pressure. In the high-pressure Raman study of $TlTiOPO_4$ (TlTP), conducted by Serhane *et al* [14], a phase transition was located close to 6 GPa where the Raman modes were found to decrease by about a factor of two. It was postulated that TlTP adopts a centrosymmetric phase which is paraelectric and closely related to the high-temperature phase. Recently, we have conducted a preliminary high-pressure structural study of the sodium-doped material $Na_{0.3}K_{0.7}TiOPO_4$ (NaKTP) and have found that it adopts the same, though more distorted, high-pressure structure as KTP through an isosymmetric transition between 5.2 GPa and 5.9 GPa [43]. As there is a large difference between the atomic masses and atomic volumes of Tl, K and Na, it is rather remarkable that the phase transition pressures should be so similar and this suggests that the framework may play the more dominant role at the transition. This notion has been given some additional support from a single-crystal x-ray diffraction study of $KTiOAsO_4$ (KTA) conducted at ambient pressure by Mayo *et al* [44]. In their study, a buckling of the framework in the vicinity of the As2 atom was identified and found to be reminiscent of the changes in the KTP structure at high pressure. This suggests that substitution of an alternative atomic species into the framework has a similar effect to pressure and may, in turn, reduce the transition pressure. Clearly then, it is important that further high-pressure structural studies are conducted on these, and other, KTP type structural analogues.

Acknowledgments

We thank Dr P A Thomas of the Physics Department at the University of Warwick for the KTP sample and for helpful discussions of the structural pseudo-symmetry. We are grateful to Mr H Vass and Mr S Duffield for their technical assistance. We thank Dr R J Angel, Dr N L Ross and Dr D A Hugh-Jones for many useful discussions, particularly regarding their related work on framework minerals, and for their helpful comments on the manuscript. This work is supported by a grant from the UK Engineering and Physical Sciences Research Council.

References

[1] Thomas P A, Glazer A M and Watts B E 1990 *Acta Crystallogr.* B **46** 333–43
[2] Tordjman I, Masse R and Guitel J C 1974 *Z. Kristallogr.* **139** 103–15

[3] Masse R and Gernier J 1971 *Bull. Soc. Fr. Mineral. Crystallogr.* **94** 437–42
[4] El Brahimi M and Durand J 1986 *Rev. Chim. Miner.* **23** 146–53
[5] Slobodyanic N S, Nagornyi P G, Skopenko V V and Lugovskaya E S 1987 *Russ. J. Inorg. Chem.* **32** 1023–6
[6] Phillips M L, Gier T E, Eddy M M, Kedder N L, Stucky G D and Bierlien J D 1989 *Solid State Ion.* **32/33** 147–53
[7] Stucky G D, Phillips M L F and Gier T E 1989 *Chem. Mater.* **1** 492–509
[8] Kourouklis G A, Jayaraman A and Ballman A A 1987 *Solid State Commun.* **62** 379–82
[9] Allan D R, Loveday J S, Nelmes R J and Thomas P A 1991 *Ferroelectrics* **124** 367–72
[10] Allan D R, Loveday J S, Nelmes R J and Thomas P A 1992 *J. Phys.: Condens. Matter* **4** 2747–60
[11] Allan D R and Nelmes R J 1992 *J. Phys.: Condens. Matter* **4** L395–8
[12] Somayazulu M S, Ramachandran H S, Sharma S M and Sikka S K 1993 *AIP Conf. Proc.* **309** 343–5
[13] Tozer S W 1993 *Rev. Sci. Instrum.* **69** 2607
[14] Serhane M, Dugautier C, Farhi R, Moch P and Pisarev R V 1991 *Ferroelectrics* **124** 373–8
[15] Adams D M, *Diacell Products*, 54 Ash Tree Road, Leicester, UK
[16] King H E and Finger L W 1979 *J. Appl. Crystallogr.* **12** 374
[17] Nelmes R J, Loveday J S, Kaldis E and Karpinski J 1990 *Physica* C **172** 311–24
[18] Finger L W and King H E 1978 *Am. Mineral.* **63** 337
[19] King H E and Finger L W 1981 *High Pressure Crystallography with a CAD4; Instruction Manual* (Delft: Enraf-Nonius)
[20] Zucker U H, Perenthaler E, Kuhs W F, Buchmann R and Schulz H 1983 *J. Appl. Crystallogr.* **16** 358
[21] Prince E and Nicholson W L 1985 *Structure and Statistics in Crystallography* ed A J C Wilson (New York: Adenine) pp 183–6
[22] Hazen R M and Finger L W 1989 *Am. Mineral.* **74** 352
[23] In this example a composition with An_{100} and $Q_{od} = 0.85$ (see [24] for definitions) was selected
[24] Angel R J 1994 *Feldspars and Their Reactions* ed I Parsons (London: Kluwer)
[25] Hugh-Jones D A 1995 private communication
[26] Hugh-Jones D A and Angel R J 1994 *Am. Mineral.* **79** 405–10
[27] Voronkova V I, Yamovski V K, Sorokina N I, Verin I A and Simonov V I 1993 *Kristallografiya* **38** 147
[28] Harrison W T A, Gier T E, Stucky G D and Schultz A J 1990 *J. Chem. Soc., Chem Commun.* **7** 540–2
[29] Thomas P A 1992 private communication
[30] Thomas P A and Glazer A M 1991 *J. Appl. Crystallogr.* **24** 968
[31] Munowitz M, Jarman R H and Harrison J F 1992 *Chem. Mater.* **4** 1296
[32] Hansen N K, Protas J and Marnier G 1988 *C.R. Acad. Sci, Paris* II **307** 475
[33] Sastry P U M 1991 *Solid State Commun.* **78** 593
[34] Zumsteg F C, Bierlein J D and Gier T E 1976 *J. Appl. Phys.* **47** 4980
[35] Crennel S J, Morris R E, Cheetham A K and Jarman R H 1992 *Chem. Mater.* **4** 82–8
[36] Munowitz M, Jarman R H and Harrison J F 1993 *Chem. Mater.* **5** 1257
[37] Christy A G 1995 *Acta Crystallogr.* B **51** 753–7
[38] Christy A G and Angel R J 1995 *Phys. Chem. Miner.* **22** 129–35
[39] Hackwell T P and Angel R J 1995 *Am. Mineral.* **80** 239–46
[40] Hackwell T P 1994 *PhD Thesis* Department of Geological Sciences, University College London
[41] Levien L and Prewitt C T 1980 *Am. Mineral.* **66** 315–23
[42] Zhang L and Hafner S S 1992 *Am. Mineral.* **77** 462–73
[43] Allan D R, Angel R J and Nelmes R J 1996 in preparation
[44] Mayo S C, Thomas P A, Teat S J, Loiacono G M and Loiacono D N 1994 *Acta Crystallogr.* B **50** 655–62